coatings

MDPI

Article

Hard Quasicrystalline Coatings Deposited by HVOF Thermal Spray to Reduce Ice Accretion in Aero-Structures Components

J. Mora [1,*], P. García [2], R. Muelas [1] and A. Agüero [2]

[1] Ingeniería de Sistemas para la Defensa de España SA, Beatriz de Bobadilla No. 3, 28040 Madrid, Spain; rmuelas@isdefe.es

[2] Instituto Nacional de Técnica Aeroespacial, Área de Materiales Metálicos, Ctra. Ajalvir Km 4, 28850 Torrejón de Ardoz, Spain; garciagp@inta.es (P.G.); agueroba@inta.es (A.A.)

* Correspondence: modsurf4.pers_externo@inta.es

Received: 17 February 2020; Accepted: 19 March 2020; Published: 20 March 2020

Abstract: Weather hazards, in particular icing conditions, are an important contributing factor in aviation accidents and incidents worldwide. Many different anti-icing strategies are currently being explored to find suitable long-lasting solutions, such as surface engineering, which can contribute to reduce ice accumulation. Quasicrystals (QCs) are metallic materials, but with similar properties to those of ceramic materials, such as low thermal and electrical conductivities, and high hardness. In particular, QCs that have low surface energy are commercially used as coatings to replace polytetrafluoroethylene (PTFE), also known as Teflon, on frying pans, as they do not scratch easily. PTFE exhibits excellent anti-wetting and anti-icing properties and therefore QCs appear as good candidates to be employed as ice-phobic coatings. Al-based QCs have been applied by High Velocity Oxyfuel (HVOF) thermal spray on typically used aeronautic materials, such as Ti and Al alloys, as well as steels. The coatings have been characterized and evaluated, including the measurement of hardness, roughness, wetting properties, ice accretion behavior in an icing wind tunnel (IWT), and ice adhesion by a double lap shear test. The coatings were studied, both as-deposited, as well as after grinding, in order to study the effect of the surface roughness and morphology on the ice accretion and adhesion properties. The QC coating was compared with PTFE and two polyurethane (PU)-based commercial paints, one of them known to have anti-icing properties, and the results indicate an ice accretion reduction relative to these two materials, and ice adhesion lower than bare AA6061-T6, or the PU paint in the ground version of one of the two QCs. Since the QC coatings are hard (GPa Vickers hardness > 5), a durable behavior is expected.

Keywords: anti-icing; quasicrystals; aeronautics; surfaces; icing wind tunnel (IWT)

1. Introduction

Ice accretion over surfaces affects many different industrial fields, such as aeronautics [1], maritime [2], aero-generators [3], power lines [4], etc., causing reduction in efficiency, energy consumption due to the required measures to mitigate it, and most significantly important, safety risks.

In particular, super-cooled water droplets present in clouds can result in the formation of an ice layer with a thickness of several millimeters in only 1 or 2 min on aircrafts. This layer is enough to modify the aerodynamic behavior of the structures [5], or disrupt the navigation systems and sensors with catastrophic consequences [6]. This phenomenon typically happens at altitudes of 1500 m to 3000 m, and temperatures from 0 °C to −20 °C, where the droplets [7] present within the clouds freeze immediately when in contact with a surface, particularly during take-off and landing at the mentioned altitudes [8].

A wide range of methods to avoid, or delay, ice accretion, and/or to release ice quickly once it has formed, are being explored. Traditionally, these methods have been grouped into two categories:

- Active methods [9]: systems that use energy to avoid ice accretion on surfaces (anti-icing mode), or favor its detachment once it has accreted (de-icing mode). Many different methods are used to this end, such as pneumatic [10], electrothermal [11], hot air heating systems [12,13], or mechanical vibration [14], among others.
- Passive methods: systems and methods based on physicochemical principles that modify the composition and/or the morphology of the surface of the component, and do not require anything of an additional energy contribution. The validated methods for use in aeronautics have been mostly based in the application of anti-freeze chemicals over the sensitive surfaces on-ground, or protect them in the first stages of flights. Most of these chemicals are anti-freezing fluids, such as some organic liquids (i. e. glycols) which reduce the freezing temperature of the water.

These active methods have some disadvantages, including adding complexity to the aircraft, weight, high-energy consumption, and the high probability of failure, whereas anti-freezing fluids are in general environmentally detrimental [15,16].

To overcome these issues, the use of anti-icing materials has attracted significant interest as a different strategy to avoid accretion or facilitate the release of ice. Different strategies have been proposed, many of them based on hydrophobic surfaces, which have commonly been associated with ice-phobicity. A large number of studies [17] have established the correlations between these two properties.

The static contact angle (SCA), and especially, dynamic wetting parameters, such as contact angle hysteresis (CAH), the roll-off angle (RoA), or the sliding angle (SA), have been related with ice-phobic behavior. The highly slippery behavior of Cassie–Baxter state super hydrophobic (SHP) materials (high CAH, low RoA or CAH), has been explored in studies, under the premise that the super-cooled water droplets should bounce and/or slide before freezing [18]. Many of these Cassie–Baxter SHP textures are based on hierarchical-structured surfaces (Figure 1) [19], inspired in bio-strategies (i.e., lotus leaf [20], rose petals [21], or the Gecko skin [22]). In these structures several levels of surface roughness, from nano- to micro-sizes, in combination with waxes with suitable chemistry, can reduce the interaction of the material and supercooled water droplets, by retaining air bubbles in the interface between both, achieving anti-icing [23] and self-cleaning properties.

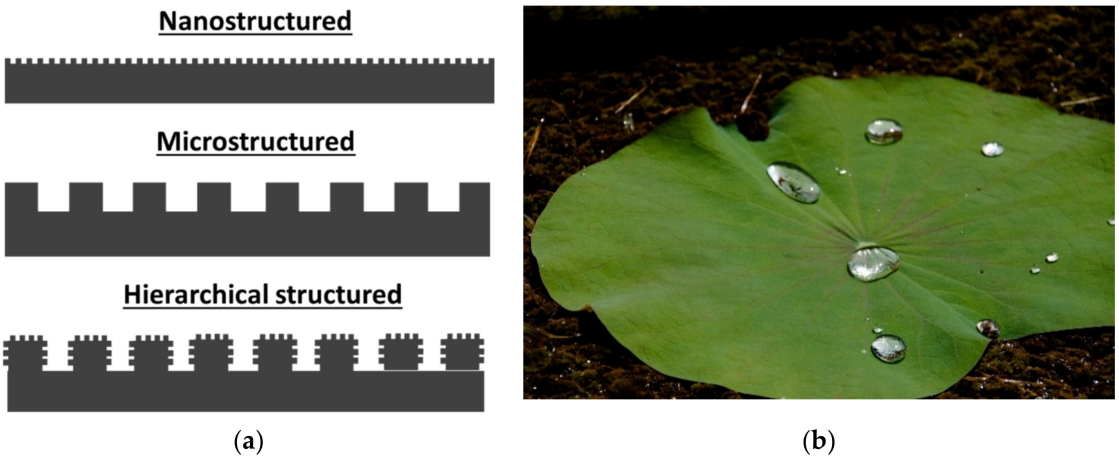

Figure 1. (**a**) Scheme of hierarchical textures formed by different levels of roughness. (**b**) Image of water repellency in the lotus leaf.

However, some other studies showed that there no clear correlation of hierarchical structures with anti-icing properties [24,25]. For instance, Jung et al. used freezing delay measurements and crystallization dynamics, and evidenced that hydrophilic surfaces with roughness values close to the

minimum incipient ice crystal radius (required to maintain the icing process) display considerably higher ice-phobicity than typical hierarchically rough SHP surfaces. This critical radius depends on external parameters, such as the temperature and humidity as falls within the nano-metric scale.

Nosonovsky and collaborators tried to find a relationship of ice-phobicity in comparison with hydrophobicity, and suggested that SHP materials are not always ice-phobic, because of the condensation of water vapor in the areas, which are not in contact with the liquid [26].

Ice adhesion is yet another critical parameter, which has been correlated with surface roughness. Most work carried out in this field show that the higher the roughness, the higher the ice adhesion [27]. Other authors have also studied the relationship between the SCA and ice adhesion, but the results do not always lead to a clear conclusion [28–30]. In fact, Zou and coworkers observed a very good correlation between SCA and ice adhesion measured as shear strength only on surfaces with similar roughness [17], whereas Kulinich and collaborators found a good correlation between adhesion and the CAH, but only for surfaces with a similar chemistry [31]. Meuler et al. studied the relationships between water wettability and ice adhesion, and concluded that any further appreciable reduction in ice adhesion strength will require textured surfaces [32]. Farzaneh and coworkers synthetized an rf-sputtered PTFE superhydrophobic coating, which achieved an ice adhesion strength 3.5 times lower than on polished aluminum [33]. Low ice adhesion values have been reported for low surface energy materials, polymers such as PTFE, or silicones.

In any case, the relationship between hydrophobicity and ice-phobicity is controversial, especially for aeronautic conditions. In addition, the static wetting laboratory measurements poorly represent in-cloud icing parameters. The typical droplet diameter used for SCA measurements is around 2 mm, or higher for RoA measurements, while in the Federal Aviation Administration 14 CFR Parts 25 appendix C [34], 20 μm droplets are described as typical. The impact speed has also high relevance, and small droplets reaching the surface at 100 m/s will not behave in the same manner as big droplets softly placed in a surface. Finally, there are no standards for laboratory ice accretion and adhesion methods.

One interesting strategy developed in recent years to reduce icing is the use of Slippery Liquid Infused Porous Surfaces (SLIPS). First reported by Aizenberg et al. [35], it is inspired on natural non-wetting structures, specifically in the Nepenthes pitcher plant [36]. Immiscible lubricant liquids are infused in porous coatings, or micro and nano structures, to lock in place the infused lubricating fluid and form a surface layer with a high level of water sliding and low ice adhesion [37,38].

A promising variation of SLIPs are the magnetic slippery surfaces (MAGSS). Peyman et al. [39] use ferrofluids [40,41] to generate a magnetic liquid–water interface with lower interfacial energy than in the solid–water interfaces. The energy barrier for ice nucleation is increased, and the ice nucleation delay time is 2–3 orders of magnitude higher than state-of-the-art ice-phobic surfaces [42,43].

In summary, although a lot of knowledge has been acquired in recent years, there is still lack of precise understanding relative to the factors governing ice accretion and in particular, how to design a surface to be ice-phobic. Several solutions have been proposed, many of them based on polymeric coatings [44,45], as silicones or fluoropolymers [46], and despite promising reductions in ice accretion or adhesion levels [47], many of them have evaluated the durability of these solutions [48,49], but up to now, no anti-icing solution that supports the restrictive requirements requested in aeronautics have been reported, and the study of durable solutions must go on.

Quasicrystalline materials (QCs) could be an attractive alternative to fight ice accretion, due to their special properties. Quasicrystals are structural forms that challenge the classical theory of crystals, as they are both ordered and non-periodic, and display symmetry orders such as 3, 5 and 10 [50]. QCs are generally brittle, preventing their use as bulk materials, but their very interesting and useful properties (Table 1) can be exploited if employed as coatings. Some interesting properties of QCs are described as follows:

- Low coefficient of friction [51]: there is published data that mainly correspond to dry scratch testing using various indenters with spherical tips, in which the values of the friction coefficient

with diamond are as low as 0.05 under constant-load operations. Friction coefficients for cemented carbide, hardened steel and alumina tips are of the order of 0.20 [52].

- High hardness [53]: in ordered metals under strain, the atomic planes or layers slide past one another (movement of the dislocations), but in non-periodic structures, so such sliding is not possible, resulting in elevated hardness. For some QC materials, values within the 10 GPa range have been measured [54], comparing favorably with the hardness levels for heat-treated, tribological steel (high-speed steels and steels used for ball bearings).
- Low surface energy [55]: some QCs present a rather low surface energy, much lower than that of a typical clean metal, and lower than that of an oxidized metal (i.e., alumina) [56]. It has been proposed that this low surface energy is (at least in part) caused by the peculiar electronic structure of the material's surface, characterized by a "pseudo-gap" (a reduction) in the density of states at the Fermi level [57]. This reduction causes a lack of empty places for electronic interactions with other surfaces or liquids as water. This pseudo-gap has been demonstrated by theoretical calculations and experimental results of Belin and Ferre, among others, and it is a universal characteristic of QCs [58].

Table 1. Properties of some quasicrystals (QCs) compared with traditional materials and alloys.

Hardness (Hv)		Coefficient of Friction (Unlubricated, with a Diamond Pin)		Surface Energy (mJ/m^2)	
Material	**Value**	**Material**	**Value**	**Material**	**Value**
Diamond	6000–10000	Copper	0.42	Iron (clean)	2480
Silica	750–1200	Aluminum alloy	0.37	Copper (clean)	1830
i-Al-Cu-Fe	800–1000	Low-carbon steel	0.32	Alumina	50
i-Al-Pd-Mn	700–800	i-Al–Cu–Fe	0.05–0.2	i-Al-Pd-Mn	24–25
Aluminum	25–45				

The combination of low friction coefficient, high hardness and low surface energy leads to anti-stick properties on some Al–Cu–Fe QCs systems. Indeed, frying pans or other cookware coated with this family of QCs have been commercialized [59]. Cooked food does not stick to the pan, which can also be vigorously cleaned without damage, as it does not scratch.

Thermal spray is a well-known, relatively low-cost coating technique which has been little explored as an alternative to deposit SHP coatings, despite its possibilities to coat large scale components. Zhang et al. applied TiO_2/h-BN composite coatings by suspension plasma spraying, which showed stable super hydrophobic behavior when the BN content was 15% [60]. Micro- and nano-scale topographies were also achieved on TiO_2 suspension plasma-sprayed coatings by Sharifi et al. [61]. Recently hard Fe-based amorphous coatings deposited by plasma spraying were studied by Qiao and collaborators, who found that depending on the spray parameters, a wear resistant triple-level hierarchical surface morphology could be obtained [62]. When these coatings were impregnated with heptadecafluoro-1,1,2,2-tetrahydro-decyl-1-trimethoxysilane, SPH behavior was observed.

Very little published work related to the anti-icing behavior of thermal-sprayed coatings can be found in the literature. Koivuluoto and coworkers studied the anti-icing behavior of polyethylene-based polymer coatings deposited by flame spraying, which exhibited low ice adhesion compared to Al alloys and steels, and outperformed painted polyurethane coatings when subjected to impact tests [63]. Xi and collaborators deposited WC-12Co by HVOF, and then modified its surface by adding a nano-SiO_2 suspension. The resulting coating was SPH, which promoted freezing delay relative to uncoated weathering steel, and exhibited low ice adhesion [64].

The objective of this work is thus to study of the behavior under icing conditions of two anti-stick QCs coatings based on Al, Fe, Cu, Cr, deposited by HVOF. For this, the following properties:

- Roughness (R_a and R_z).
- Static contact angle (SCA), contact angle hysteresis (CAH) and Roll-off angle (RoA)

- Ice accretion.
- Ice adhesion.

Have been investigated and compared with four reference materials:

- Al alloy AA6061 T6 commonly used in aeronautics.
- PTFE, a well-known anti-wetting, and anti-icing material, but with low hardness and strength, as well as a high wear rate, which limit its application in this field [65].
- Two commercially available polyurethane (PU) paints, certified to for aeronautical use in commercial aircrafts. One of them is not commercialized as anti-icing, but was used by Airbus during the studies carried within the EC project STORM, showing significantly reduced ice adhesion with respect to, e.g., bare metallic surfaces like titanium or aluminum [66]. The other one is an aeronautical standard paint without reported anti-icing properties.

2. Experimental Methods

2.1. Materials

Coupons of the required sizes for each of the tests were cut of AA6061 T6 (0.66% Si, 0.11% Mn, 0.18% Cr, 0.23% Cu, 0.41% Fe, 0.86% Mg, 0.06% Zn and 0.03% Ti) provided by ThyssenKrupp Materials Iberica. PTFE plate (thickness of 3 mm) was acquired from J. Morell S.A (Tarragona, Spain).

The aeronautic PU paint FS-37925 WHITE MATT (PEXA) was obtained from the Industrial Association of Navarra (AIN) (Navarra, Spain), whereas the PU paint Alexit 414-44 with anti-icing behavior, was provided by Mankiewicz.

The characteristics of the two anti-stick QCs powders, QC1 and QC2 for short, are shown on Table 2. The powders were prepared by atomization. They exhibit spherical geometry (Figure 2), and its composition as measured by EDS is uniform.

Table 2. Powders employed to deposit the corresponding coatings by High Velocity Oxyfuel (HVOF).

Denomination	Company	Powder Size (μm)	Composition (wt %)	Commercial Name
QC1	SAINT GOBAIN	+20 −75	54.1 Al; 17.9 Cu; 13.7 Fe; 14.3 Cr	CRISTOME A1/S
QC2	SAINT GOBAIN	+25 −63	48.8 Al; 40.2 Cu; 19.1 Fe + 0.9 B	CRISTOME F1

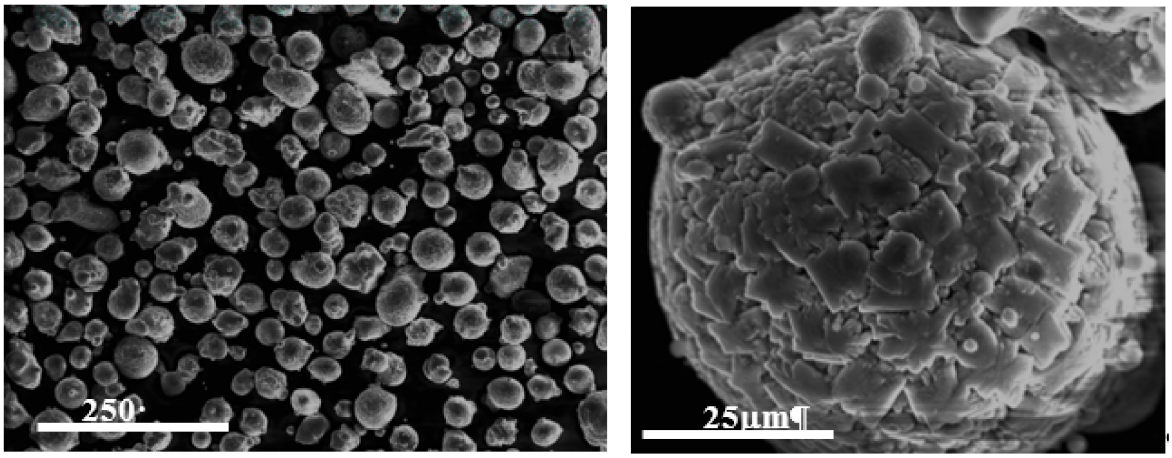

Figure 2. Field Emission Scanning Electron Microscope (FESEM) images of atomized QC powders employed to produce the coatings.

2.2. Coating Application

All paints and coatings were deposited on both sides of AA6061 T6 coupons. The PU PEXA paint was applied by dipping and curing, following the provider instructions.

The PU Alexit paint was applied by Technology Partners (TECPAR) (Warsaw, Poland), using a spray gun and cured following the provider instructions.

Regarding the thermal spray process (Figure 3), the specimens were grit blasted and degreased with Acetone (Sigma-Aldrich ACS reagent, ≥99.5%) in an ultrasonic bath, prior to coating. The powders were pre-heated at 80 °C and mixed for 2 h by means of a Glass-Col stirrer (model 098ARD9924, Terre Haute, IN, USA) before the deposition. This process is needed to obtain completely dry powders and to assure the correct flow. The powders were sprayed employing a Sulzer Metco Diamond Jet Hybrid HVOF unit (A-3120) mounted on a six-axis robot (ABB), and fed by a twin rotation powder feeder. The corresponding spraying parameters are shown in Table 3.

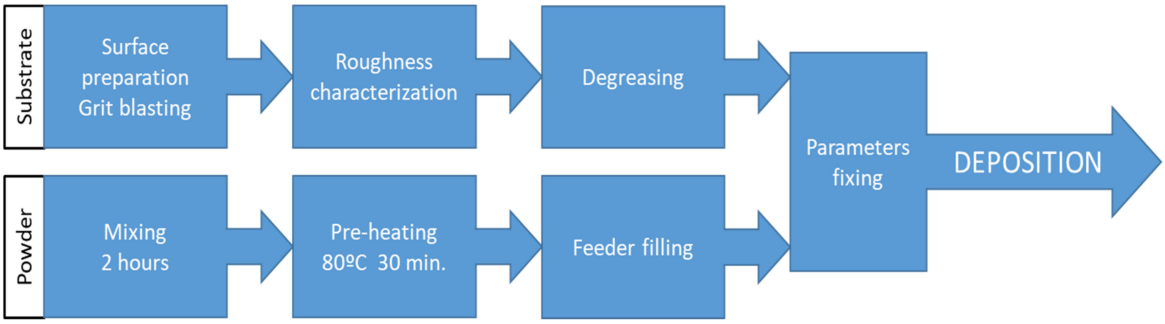

Figure 3. Scheme of the previous processes to HVOF deposition.

Table 3. HVOF Spray Parameters.

Denomination	Oxygen (l/min)	Hydrogen (l/min)	Nitrogen (l/min)	Powder Feeder Rate (g/min)	Spray Distance (mm)	Transverse Speed (mm/s)
QC1	180	344	635	25	360	1691
QC2	214	344	635	25	300	1691

Regarding to the surface preparation prior to testing, both the AA6061 T6 and PTFE used as references for the study were used as received, after cleaning with water and degreasing with iso-propanol (ACS reagent, ≥99.5%). The two PU sprayed coatings were employed in the "as deposited" condition.

The QC coatings were tested both in the "as sprayed" state, and after grinding with a gradual process with P-180, P-350 and P-600 SiC papers.

2.3. Coating Characterization

2.3.1. Microstructure

The coatings were characterized by Field Emission Gun Scanning Electron Microscopy (FESEM) (JEOL JSM-6500F (Tokyo, Japan) equipped with an Oxford INCA 200 EDX/WDX micro-analyzer) from polished cross sections before and after exposure. Phase composition was examined by Xray diffraction (XRD) in a Philips X'Pert equipment using the Cu Kα line (0.15418 nm). Thicknesses were determined by a minimum of 20 measurements and their average were reported in the text. The topographic images were obtained with a Leica digital microscope (DVM6) from (Wetzlar, Germany).

2.3.2. Roughness

The surface roughness was measured using a profilometer Time3200 model TR200 from Tecnimetal S.A. (Madrid, Spain). Five measurements of R_a, and R_z were made in representative parts of every material, following the UNE-EN ISO 4287:1999/A1:2010 standard.

2.3.3. Wetting Behavior

These properties were evaluated with an Optical tensiometer (Biolin scientific Theta lite) from Lasing, S.A. Madrid (Spain), using a volume of 5 µL of deionized water for the SCA, and 10 µL for RoA, and CAH. RoAs and CAHs were determined using the tilted plane method [67], at a fixed rate of 2°/s. Three measurements were made to obtain the mean value.

2.3.4. Hardness

Vickers microhardness was measured according to ISO-6507-1, using a Future Tech FM system, from 10 evenly spaced indentations on the cross section of the coatings (minimum thickness of 100 µm), employing a 300 g load.

2.4. Icing Wind Tunnel (IWT) Testing

An open section wind tunnel (Figure 4) was employed for the ice accretion evaluation. It is located inside a 54 m^3 cold climate chamber that allows temperature stability during long duration tests. The precooled samples (140 × 25 × 3, 3 mm) were fixed in the center of the test chamber (15 × 15 cm^2), with the coated face perpendicular to the air flow. The exposed area of the samples was 25 cm^2.

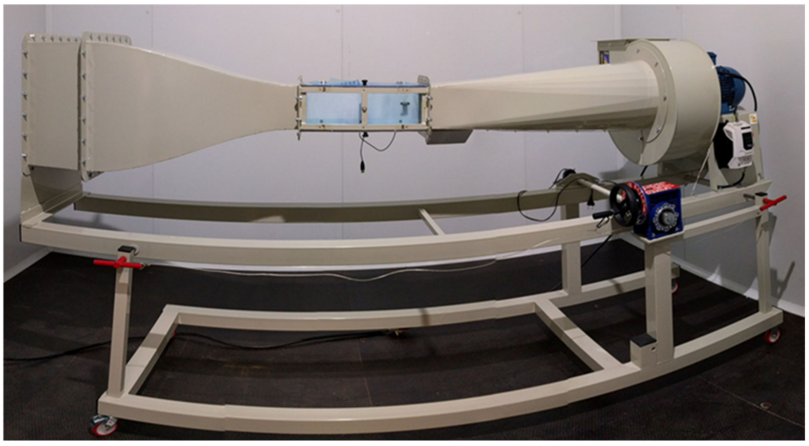

Figure 4. Icing wind tunnel.

Two representative icing conditions were simulated: glaze ice and rime ice (Table 4), and the corresponding parameters are gathered in Table 4.

Table 4. Test conditions for glaze and rime ice.

Conditions	Glaze Ice	Rime Ice
Wind speed (m/s)	50	50
Temperature (°C)	−10	−20
MVD (µm)	20	20
LMC (g/m^3)	0.5	0.5

The wind speed was measured using a Pitot probe PCE-PFM 2 taking representative values in the testing area. The used probe measures from 1 to 80 m/s, with an accuracy of 2.5%. The median volume diameter (MVD) was determined using a Malvern Spraytec system (Figure 5), provided by

IESMAT (Alcobendas, Spain), equipped with a 300 mm lens to measure droplets from 0.1 to 900 µm, and determine MVD from 0.5 to 600 µm in sprayed atmospheres, with an accuracy better than 1%. The liquid water content (LWC) was calculated using the icing blade method described in SAE ARP 5905:2003 (R2015): "Calibration and Acceptance of Icing Wind Tunnels" [68].

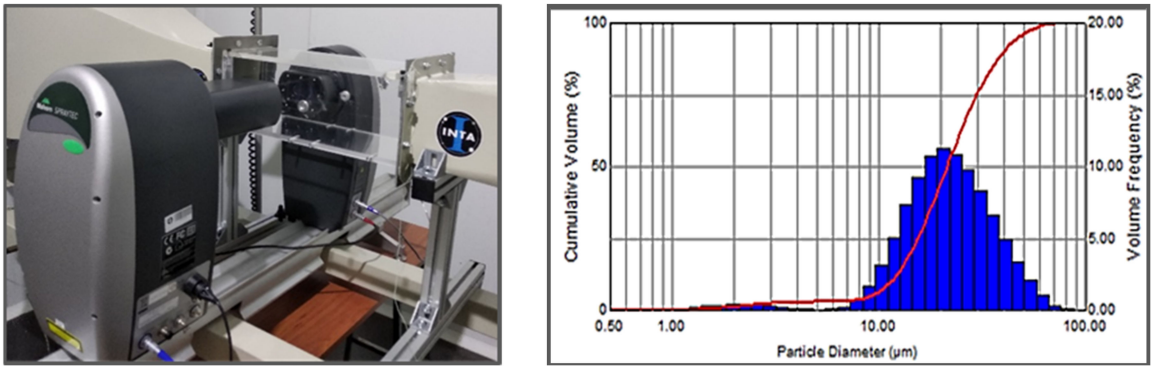

(**a**) (**b**)

Figure 5. (**a**) Image of the Spraytec system attached to the icing wind tunnel (IWT) and the testing chamber. (**b**) Droplet size distribution of the testing conditions.

Five one-minute trials of each sample were performed in each condition (rime and glaze), and the ice accretion was evaluated by direct weight measurement (difference before and after the test). The mean values of the five measurements were compared with the respective of all materials.

2.5. Ice adhesion by Double Lap Shear Test (DLST)

An Instrom 5882 Universal Machine (Barcelona, Spain) with a 5 KN loading cell placed inside a climate chamber (refrigerated with liquid nitrogen) was used. The loading cell was calibrated in the 5%–95% range. The ice layer on the surface of the coupons was formed inside an ultra-low temperature freezer (Arctiko ULTF serie)

Test Procedure

The day before the test, ice must be formed on the samples employing the following procedure: initially, the sides of the test block are sealed with transparent adhesive tape to prevent water from escaping, then the mold is filled with water, ensuring that there are no air bubbles, and finally, the specimen is placed inside ensuring that the level of water on both sides of the specimen is the same, reaching 6 mm below the top edge of the mold (Figure 6a). The so-prepared molds are then placed in a low temperature fridge at −10 °C (Arctiko ULTF series) and left for at least 16 h before the test. One hour before the test, the adhesive tape is removed, and any rest of ice accreted over the sample edges is carefully, but quickly, removed using a blade. The molds are placed again in the freezer for one more hour.

The test block is then fixed to the universal machine, previously cooled to the test temperature (Figure 6b). The samples must be moved very fast from the freezer to the test rig to avoid loss of temperature in the system, and after the selected test temperature is reached in the chamber, the samples are left for five more minutes before beginning the test.

The displacement speed is set, and the test initialized until the sample is completely out of the mold.

Plots of the measured load (N) as a function of displacement (mm) are obtained during the test, and the maximum load peak is the load needed to overcome the adhesion strength, therefore a measure of the adhesion between ice and the surface of the sample in the corresponding ice accretion conditions. Three specimens of every coating were tested to obtain the mean value and the standard deviation.

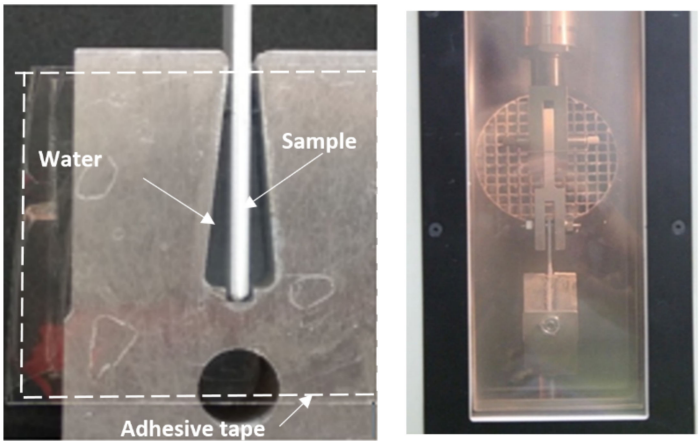

(**a**) (**b**)

Figure 6. (**a**) Test block employed to form ice on both sides of the sample. (**b**) Block attached to the Universal machine ready to start a test.

3. Results and Discussion

3.1. Characterization of the Coatings

The two chosen anti-stick QC coatings, identified as QC1 and QC2, have different contents of Al, Fe, Cu and/or Fe. Thick layers (100–150 μm) were deposited to ensure enough thickness for mechanical grinding, if needed. Both coatings showed a similar microstructure, with uniform coverage and homogeneous composition (measured by EDS), along with the presence of features typical of thermal-sprayed coatings, such as unmelted particles and pores (Figure 7). Micro-cracks were also observed, very likely as a result of the brittleness of these QC materials. Micro-cracking releases stresses in the coating, and has not shown to have a negative effect on the overall properties, such as corrosion resistance, erosion, etc. in an Al–Fe–Co–Cr QC coating, which was evaluated as a thermal barrier coating [63] Moreover, even when subjecting the said coatings to thermal cycling, the micro-cracks did not propagate into the substrate.

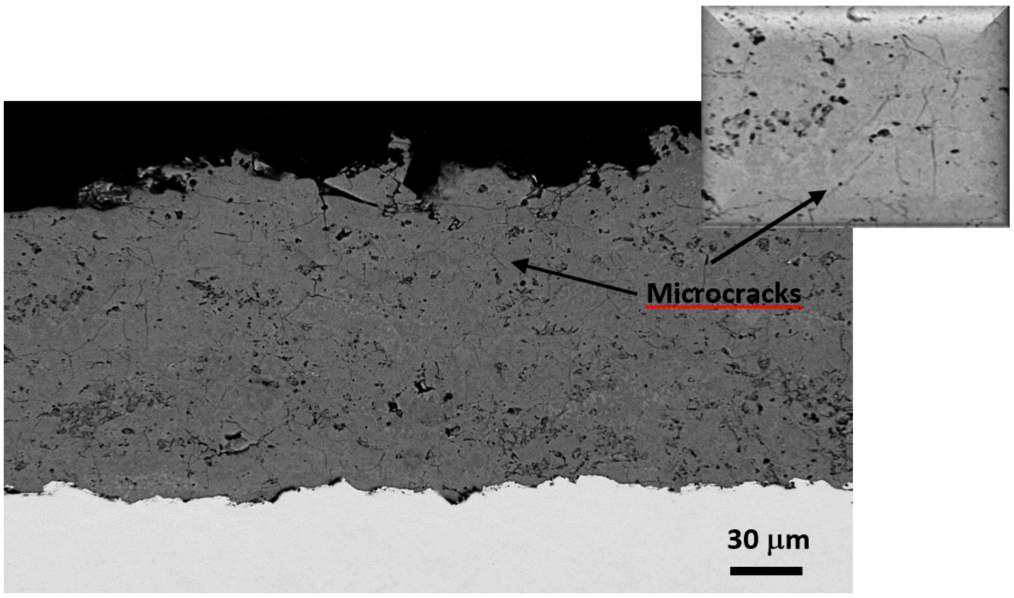

Figure 7. FESEM cross section image of one of a QC coating deposited by HVOF.

Hardness is not a property that influences ice-phobicity, but may certainly affect its durability, and as mentioned, QCs are usually harder than other metallic alloys. In fact, the hardness of the tested QC coatings, comparing with values of the references obtained in published works, is 4–6 times higher than that of AA6061 T6, and one or two orders of magnitude higher than that of the polymeric materials (Figure 8). As already discussed, the surface finishing and/or texturing of the material can be critical for obtaining ice-phobicity, and if the material is hard, ice-phobic textures may be maintained for longer periods, as they are less affected by wear, such as scratches, rain erosion etc., which is likely to occur on aeronautic surfaces. Indeed, durability is certainly one of the main current issues affecting ice-phobic materials and hard, wear-resistant surfaces could increase the durability of the ice-phobic behavior by eliminating, or at least reducing, ice nucleation sites originated by scratches.

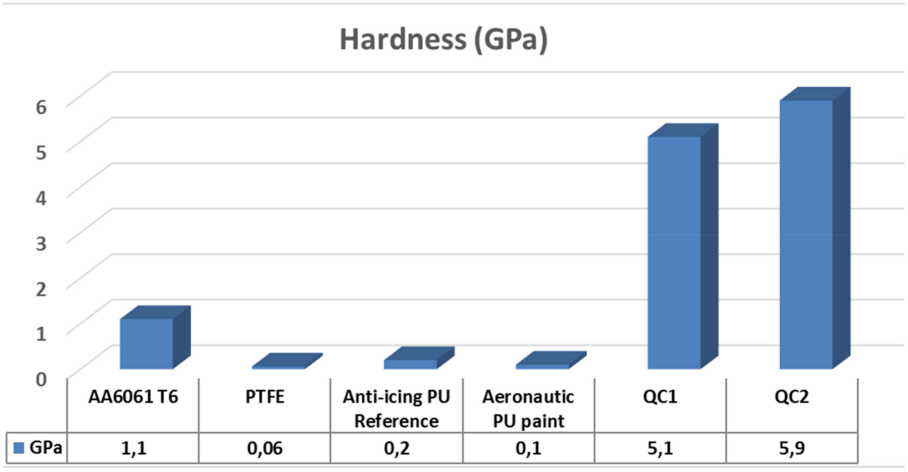

Figure 8. Vickers microhardness measured in all tested materials.

Roughness is an important parameter for ice accretion and adhesion, and thermally sprayed coatings are usually very rough (R_a: 5–20 µm, R_z: 20–100 µm). As already mentioned, in order to properly compare the wetting/sliding behavior of different materials, their roughness should be the same. Therefore, samples of each QC coating were mechanically ground to achieve the same level of R_a and R_z, than the materials used as reference as shown in Figure 9. Very low values were achieved on the two QCs coatings after grinding, which were very close to those obtained on the PU coatings, as well as the as-received AA6061 T6 alloy, and even lower than that of the as-received PTFE.

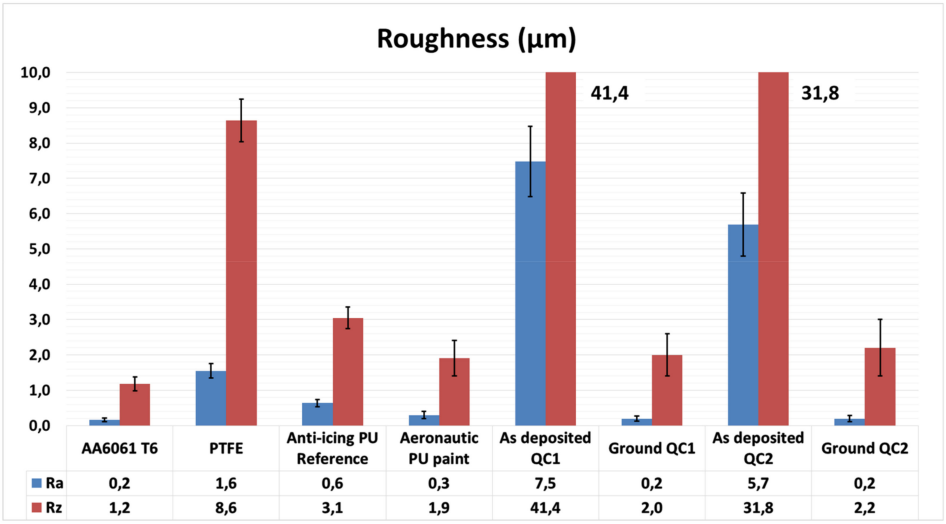

Figure 9. R_a and R_z values.

The surface images and the topography of the two coatings before and after grinding are shown in Figures 10 and 11, respectively. At low magnification, the surface of the as-deposited QC1 coating appears slightly rougher in agreement with the measured values and with some larger diameter particles, when comparing with QC2. The higher magnification images exhibit protrusions formed by conglomerates of particles with sizes significantly lower (≤5 μm) than that of the starting powders (20–75 um), clearly indicating melting and recrystallization of the material. Large holes and small pits (<5 μm in diameter) that can trap air were also detected. A hierarchical morphology was present, as particles with sizes lower than 1 μm were abundant.

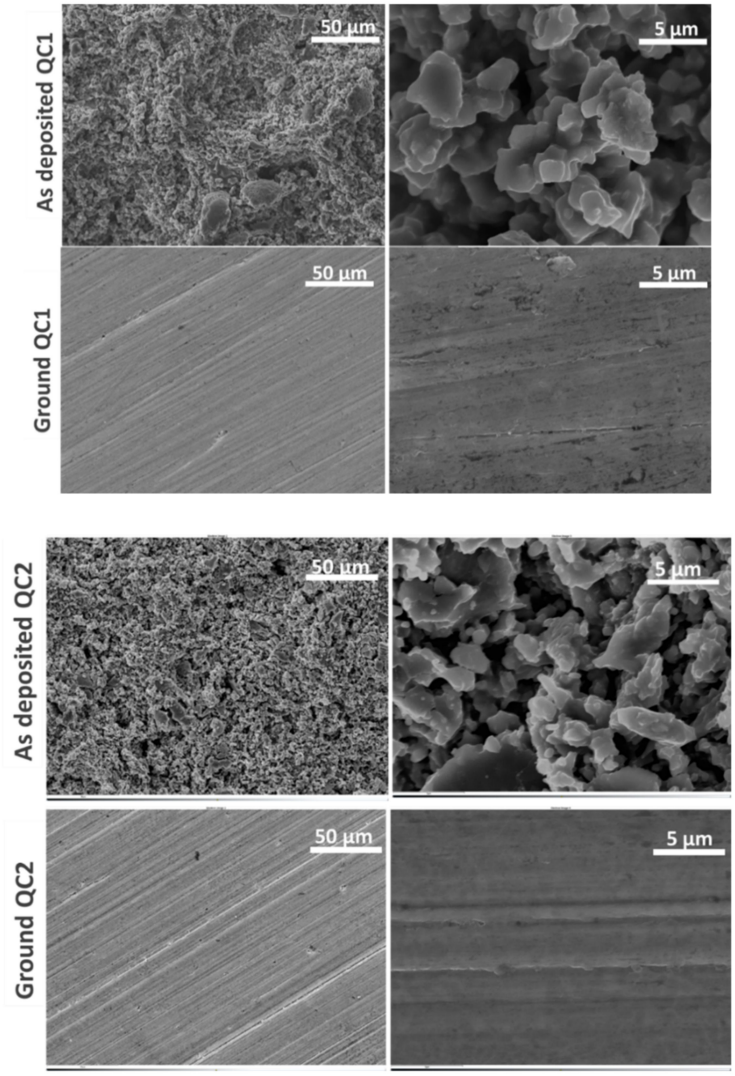

Figure 10. Scanning electron microscopy (SEM) images of surface of QCs before and after grinding.

After grinding, grooves form grinding marks were the only remarkable features that could be observed in both QC coatings, along with some pores, particularly present on QC1.

The 3D topographical images shown on Figure 11 confirm the higher roughness of the as-deposited QC1 evidencing peaks and valleys typical of thermal-sprayed coatings. The images of the uncoated AA6061 T6 substrate and PTFE are quite similar to that of the two ground QC coatings.

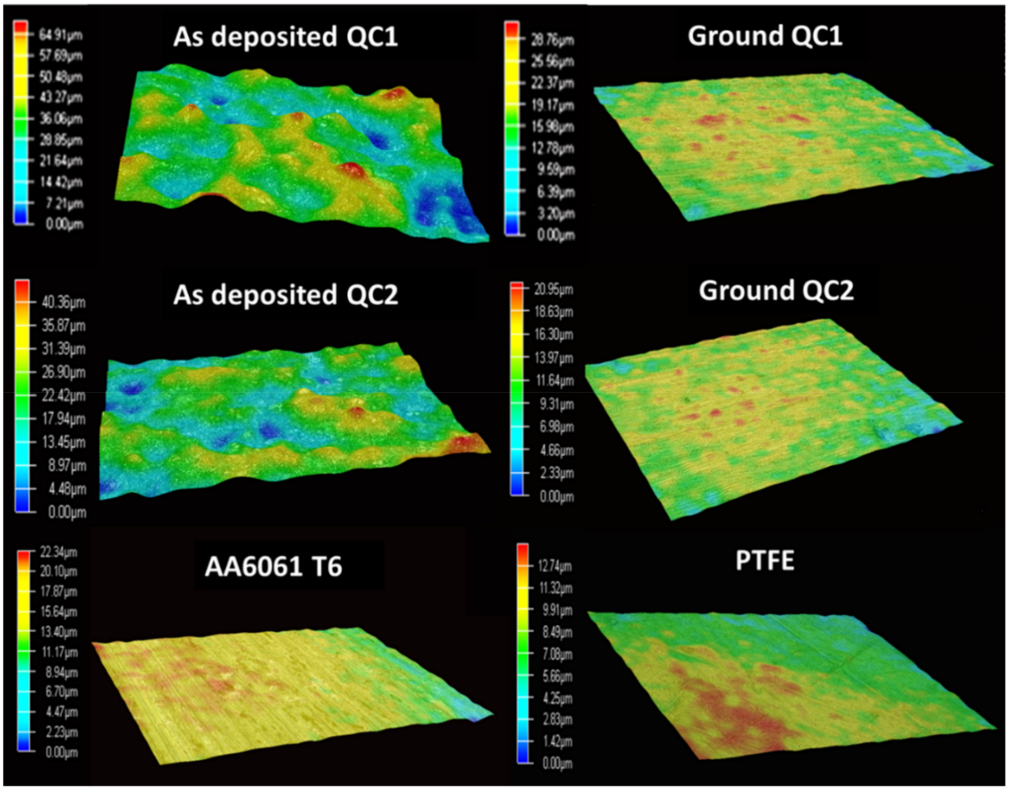

Figure 11. 3D topographical images of the QC coatings as well as the reference materials AA6061 T6 and polytetrafluoroethylene (PTFE).

The wetting properties of the reference materials and the QC coatings were evaluated by SCA and CAH measurements (Figure 12). The SCA of the two PU-based paints and the AA6061 was low, as it was expected in those materials, while on PTFE it was slightly higher, but far from the SHP range, as anticipated for a smooth PTFE.

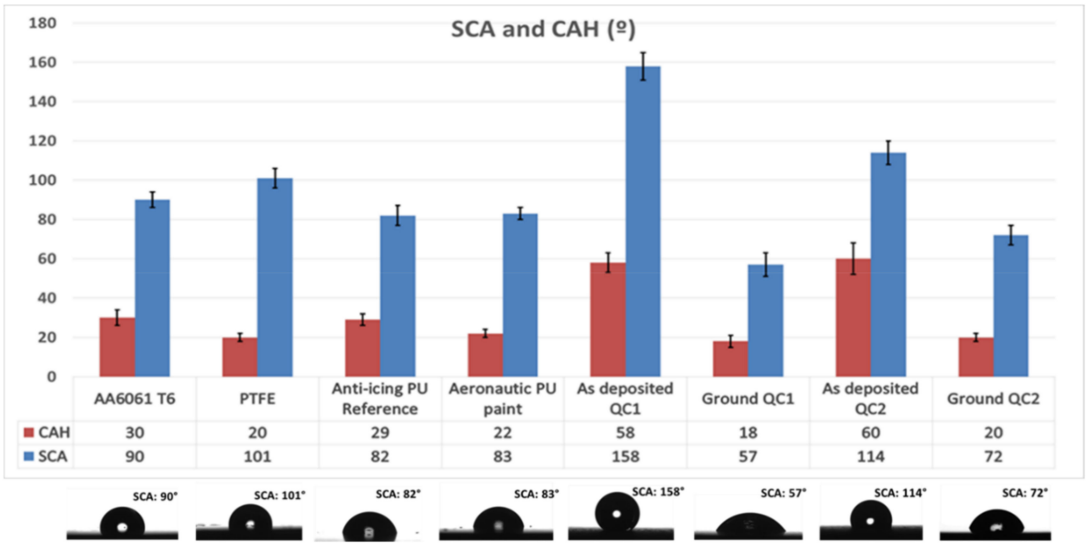

Figure 12. Static contact angle (SCA) and contact angle hysteresis (CAH), of the studied samples. The roll-off angle (RoA) of all samples was higher than 55°.

The term of "superhydrophobicity" is controversial, sometimes related with just the SCA, and other times with other wetting parameters, as CAH or RoA. In this work, we will refer to the first definition, SCA > 150°.

In contrast, the as deposited QC1 coating exhibited an SHP behavior with a SCA significantly higher than that of any of the other studied materials and coatings, even surpassing that of PTFE. QC2 also displayed a high SCA, but lower than that of QC1, falling within what is considered as hydrophobic behavior. A plot of SCA vs roughness shown on Figure 13shows a certain tendency, indicating that the highest the roughness, the highest the SCA, as expected, but it is not always the case as AA6061 T6 with the lowest measured roughness (R_a: 0.2 µm) exhibited hydrophobic behavior, whereas ground QC1 and QC2 with the same roughness, were hydrophilic.

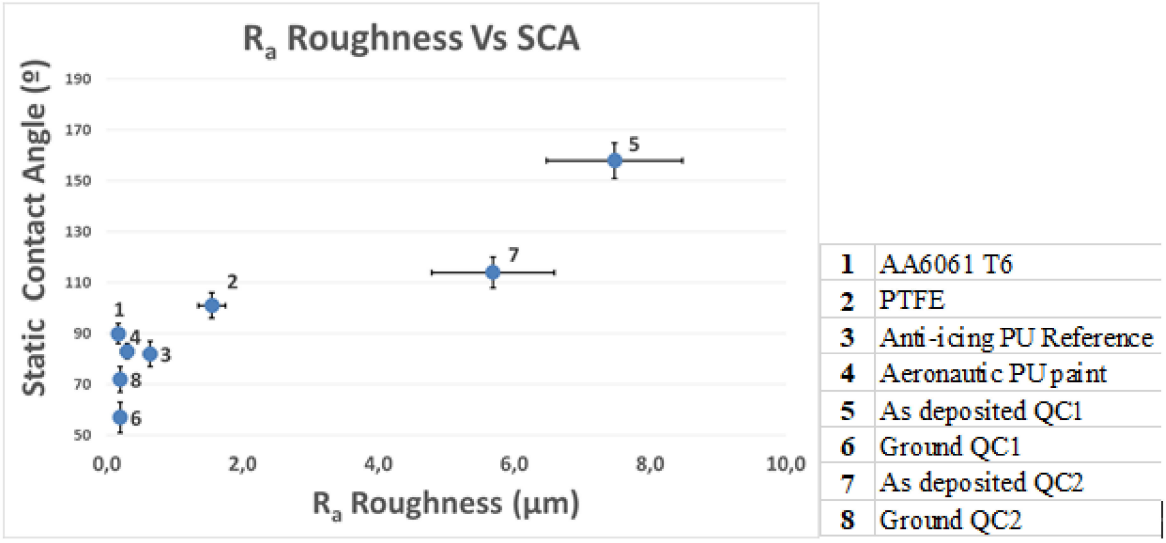

Figure 13. SCA vs Ra roughness for the studied materials and coatings.

On the other hand, the two ground QCs exhibited the lowest CAHs, together with PTFE. Since the texturing effects have been removed, this may be likely due to the low surface energy of these materials. However, none of the studied materials act in the Cassie–Baxter state (heterogeneous regime) as all of them present RoAs higher than 55°, rather showing correspondence with the Wenzel state (homogeneous regime), in which the water penetrates into the grooves and pits of rough materials (Figure 14). In the case of the QCs, this may be due to the presence of grinding grooves.

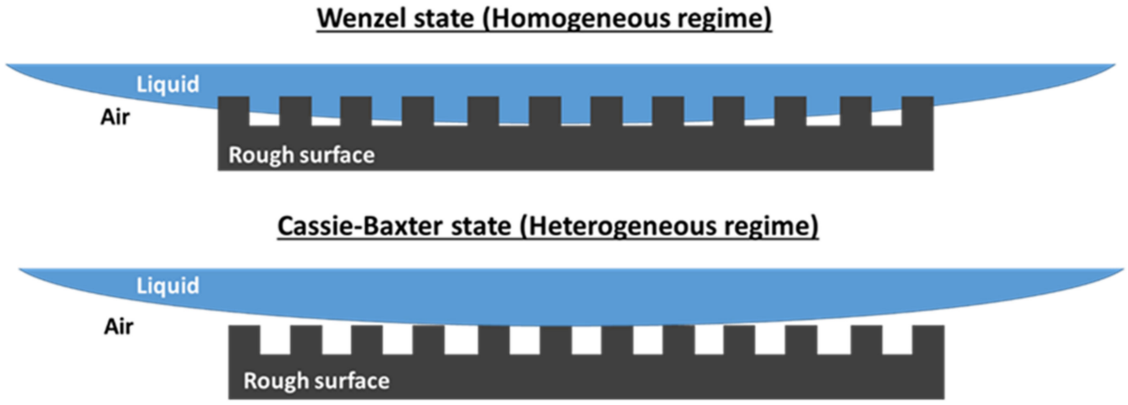

Figure 14. Cassie–Baxter and Wenzel states (heterogeneous and homogeneous regime).

The measured SCA on PTFE (101°) was slightly lower than the maximum reported value, which are in the order of 110° [69], likely caused by dissimilar finishing. PTFE is known as an anti-stick

and anti-icing material, but it is not superhydrophobic, showing that this property is not necessarily needed to have anti-icing behavior [26,30].

3.2. Ice Accretion

The samples were exposed to two types of ice, rime and glace, which are typically formed in clouds. The test conditions to obtain them are described in Table 4.

3.2.1. Rime Ice

Rime ice (Figure 15) is a granular, rough, opaque and whitish-looking ice formed by the rapid freezing of super-cooled drops after hitting a surface. The rapid freezing speed causes the air to be trapped inside the ice, giving it a whitish appearance, and making it porous and brittle. This type of ice is easier to remove than compact ice, and more easily detected [34].

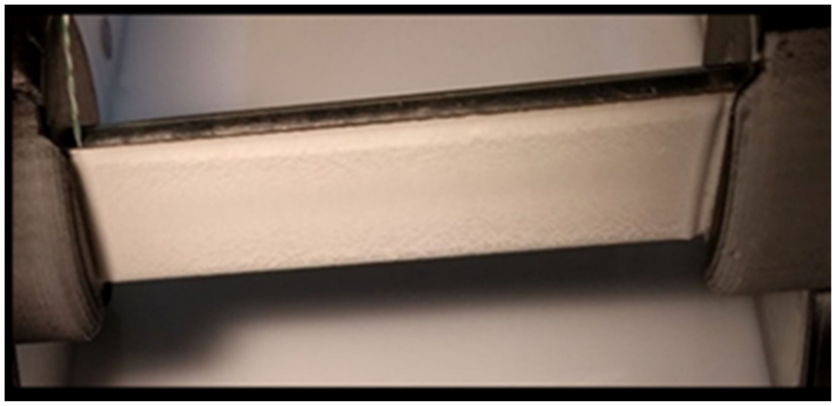

Figure 15. Image of rime ice obtained in the IWT on flat sample profiles.

The ice weight acquired by the different tested materials under conditions leading to rime ice are summarized in Figure 16. In the present test conditions (1 min of exposition to icing condition over the tested area), the differences in the rime ice-accreted mass were not so large. Many of the studies found in the published literature are focused in the aerodynamic influence of the accreted ice over aeronautic profiles, i.e., NACA 0012, or in the reduction of the energy supply of an active system in combination with an anti-icing solution (i.e., superhydrophobic coating) [70,71]. Low differences in ice accretion in the IWT of different materials has been also reported previously by Morita et al., where the very demanding conditions decrease the behavior differences among different materials [72]. Erbil et al. found an ice accretion reduction of 27 % by Teflon when compared to Cu [73]. With other metals, the reduction was even lower. Sharifi et al. [74] showed an ice accretion reduction of 49% in an SHP plasma spray coating, respecting an uncoated steel substrate, using an air velocity of 23 m/s, 0.5 g/m^3 and MVD: 30 μm. The same test, but using a 45 m/s velocity achieved a 13% ice accretion reduction. In the present case 50 m/s were employed, as it is closer to real wind velocities when flying. In any case, it is very difficult to compare the results of different tunnels, as there is no standard tunnel or methodology and the variety of parameters is very bigger.

On the basis of the results, three groups of materials can be identified: 1) PTFE and the as-deposited QC1 with the lowest ice accretion, 2) ground QCs and anti-icing PU paint with intermediate behavior and 3) as-deposited QC2, PU paint and AA6061 T6 with the highest ice accretion. The ground QC2 behavior was between intermediate and high ice accretion. Despite exhibiting a low CAH, the anti-icing behavior of the PU paint is rather poor in the present IWT, once more confirming the lack of direct correlation between the sliding properties and the anti-icing behavior. In addition, the best performing materials had very different roughness (R_a: 1.6 and 7.5 μm for the two best performing materials, PTFE, and the as-deposited QC1, respectively).

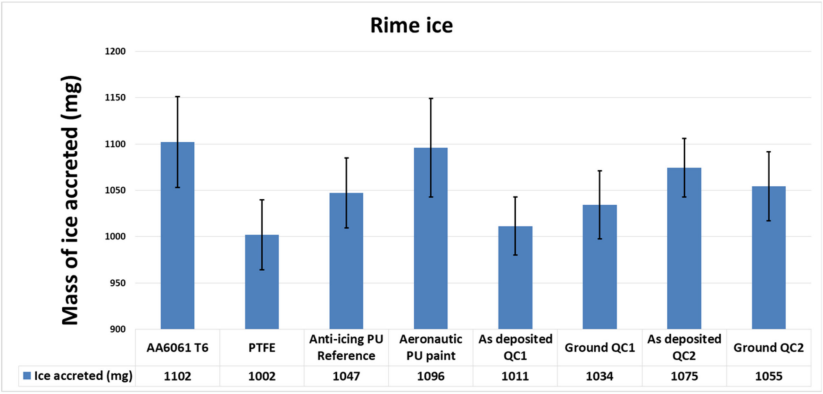

Figure 16. Ice accretion of all studied materials obtained under rime ice conditions.

The two QC coatings (as-deposited as well as ground) grew less ice than AA6061 T6, but only the as-deposited QC1 accreted low amounts of ice with a similar behavior than PTFE. Again, the lower CAHs of the ground QCs that accreted more ice cannot be correlated with the anti-icing behavior in this case.

In summary, the differences in the icing behavior of all the tested materials is not very high, and none of the wetting/sliding properties can be correlated with the observed anti-icing behavior, not even when the materials with similar roughness were compared as slight differences in the behavior were observed. It is however interesting to point out that a metallic material such as QC1 exhibited similar behavior than PTFE, which is known as a good anti-icing material.

3.2.2. Glaze Ice

Glaze (Figure 17) is a transparent or translucent ice that is formed by drops of super-cooled water, that when hitting the surface, do not fully freeze immediately. It is a denser/heavier and harder ice, more difficult to break, and usually more transparent than rime ice, and therefore more difficult to detect, consequently implying higher danger that rime ice. It is also more adherent (and therefore harder to detach), and modifies largely, the profile of the components on which it forms, affecting the corresponding aerodynamics. The Federal Aviation Regulations (FARs) point out in their Aeronautical Information Manual (AIM) that the main factors that stimulate nucleation of this type of ice are those that promote slow dissipation of the fusion heat, such as slight super-cooling and rapid accretion [34].

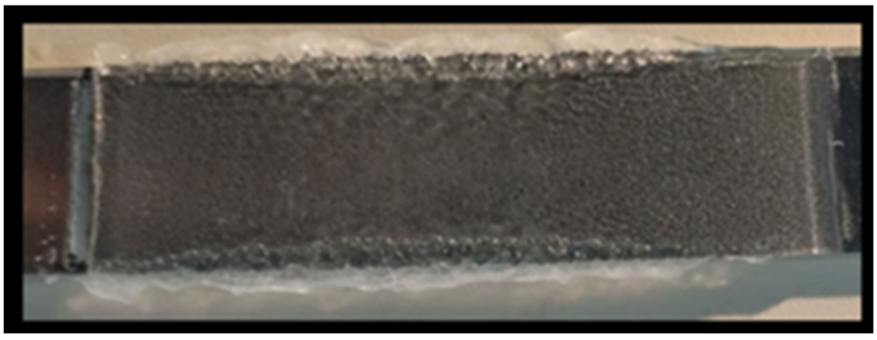

Figure 17. Image of glaze ice obtained in the IWT on a flat sample.

The results obtained in the IWT under glaze ice conditions are summarized in Figure 18. Interestingly, more mass of glaze than rime ice was accreted in general for the same test duration and exposition area. This result could be explained by the fact that, as mentioned, rime ice is porous and has a lower density (Table 5) [75].

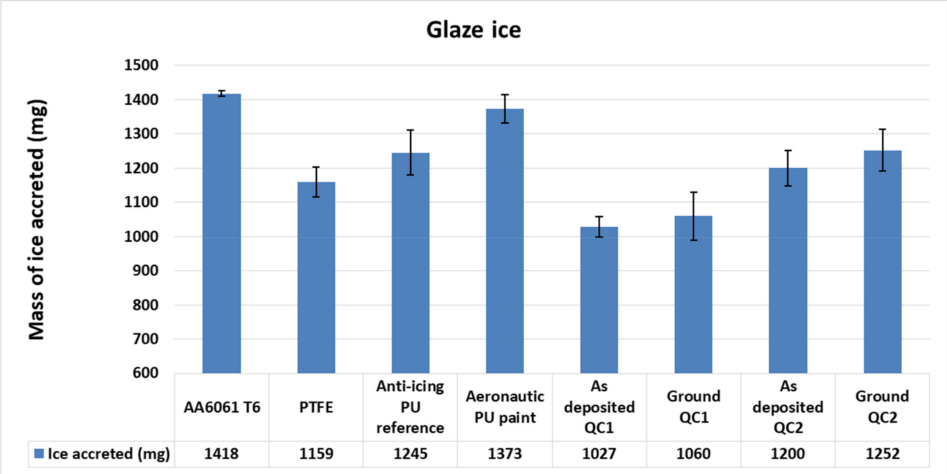

Figure 18. Ice accretion of all studied materials obtained under glaze ice conditions.

Table 5. Density of ice types, after ISO 12494:2017 [75].

Type of Ice	Density Range (kg/m^3)
Glaze	900
Wet snow	300–600
Hard Rime	600–900
Soft Rime	200–600

With glaze ice, the weight gains were again not very high, but in this case the differences between all of the materials were slightly higher. A tendency was observed, indicating that the as-deposited QC1 showed the best results, and in general, all as-deposited or ground QCs exhibited better or approximately the same anti-icing behavior than PTFE and the anti-icing PU reference.

QC1 exhibited the highest SCA, and the best result in glaze ice, so related with the flow of water over the surface before freezing. Antonini supported the good behavior of SHP materials with glaze ice [76], but in that case, an active system was involved.

As with rime ice, roughness does not seem to affect the results, as both as deposited and ground QCs show similar behavior, despite having quite different roughness. The same applies for the SCAs, with a hydrophilic material, such as ground QC1, exhibiting better anti-icing behavior than hydrophobic PTFE.

In general, the present results show that icing does not necessarily correlate with roughness and the materials wetting properties. It is therefore dangerous to use these parameters when studying new materials and surface textures as criteria to establish promising anti-icing behavior.

Anti-stick QC coatings deposited by HVOF thermal spray appear as an interesting alternative for surfaces requiring super hydrophobicity, and also for reducing ice accretion. They do not require extra surface treatments, such as impregnation with low surface energy materials, e.g., stearic acid, PTFE, etc. This may be due to the intrinsic low surface energy of these materials, which are also hard, so the durability of the surface textures is likely to be high. Work is in progress in that respect.

3.3. Ice Adhesion

The employed testing methodology is a modification of the ice adhesion by double lap shear test (DLST) used by CRREL [77], adapted to evaluate ice adhesion for aircraft anti-icing solutions. To this end, modifications such as temperature range, loading rate and the geometry of the moldsm where implemented. Although ice is generated under static conditions (in a freezer), the test has some advantages that include ease of execution, fast and easy interpretation of results and simple specimen geometry (flat samples).

The results showed on Figure 19 indicate low ice adhesion on PTFE and the Anti-icing PU reference, as expected. On the other hand, high values for AA6061 T6 and the Aeronautic PU paint were obtained, justifying the need to improve the anti-icing behavior of commercial aeronautic surfaces.

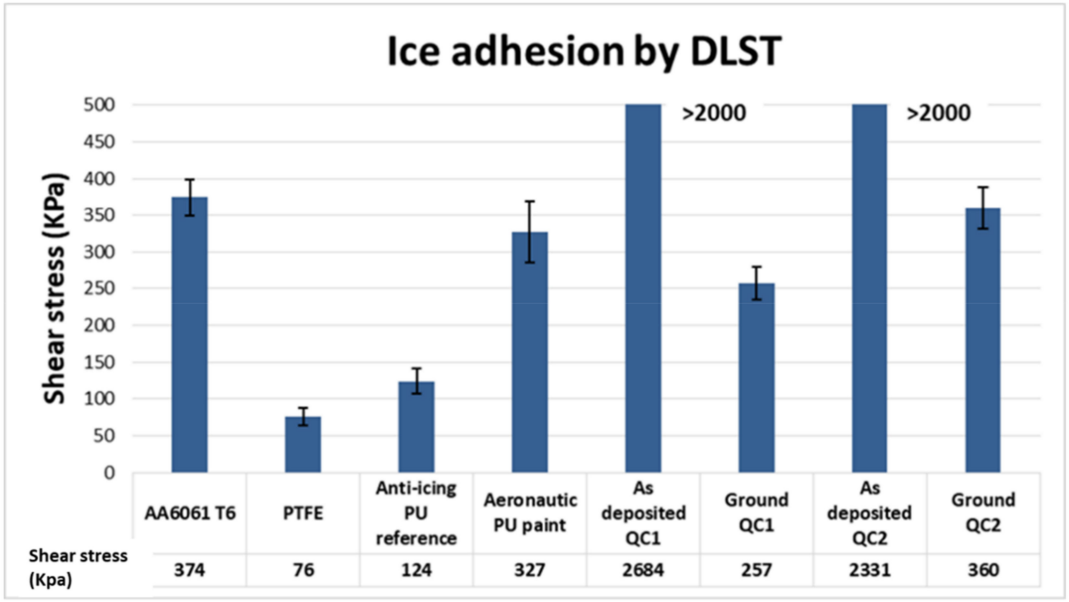

Figure 19. Ice adhesion results.

Low ice adhesion of PTFE, or PTFE-based coatings, has been reported by many authors using different ice adhesion testing methodologies [78–80].

The rough "as deposited" QCs showed very high ice adhesion, clearly influenced by the interlocking effect caused by the high roughness, as Chen et al. among others pointed out [81]. This is especially true in those ice adhesion tests, where ice formation is undertaken by a non-impact methodology. In an impact ice formation methodology, Yong et al. established for rough surfaces that surface features, that are spaced closer together and exhibit higher capillary pressure, and therefore resist droplet penetration and maintain in a Cassie–Baxter state, resulting in lower ice adhesion [26].

On the other hand, the ground versions exhibited a drastically lower ice adhesion than the as-deposited versions, but not to the level of PTFE or the anti-icing PU paint. In fact, ground QC1 exhibited lower adhesion than AA6061T6 and the Aeronautic PU paint. This is a promising behavior for a metallic material, but one that still requires improvement in order to match the very low adhesion shown by PTFE.

Roughness is without doubt a critical parameter for ice adhesion, but for low roughness values (≤1.6 Ra), there is no correlation, as PTFE with 1.6 Ra exhibits the lowest adhesion when comparing with the other lower roughness materials (Figure 20). This indicates that the chemical composition and the corresponding electronic interactions with the ice layer are also relevant. The reported low surface energy of ground QC1 could be behind the lower ice adhesion when comparing with AA6061 T6.

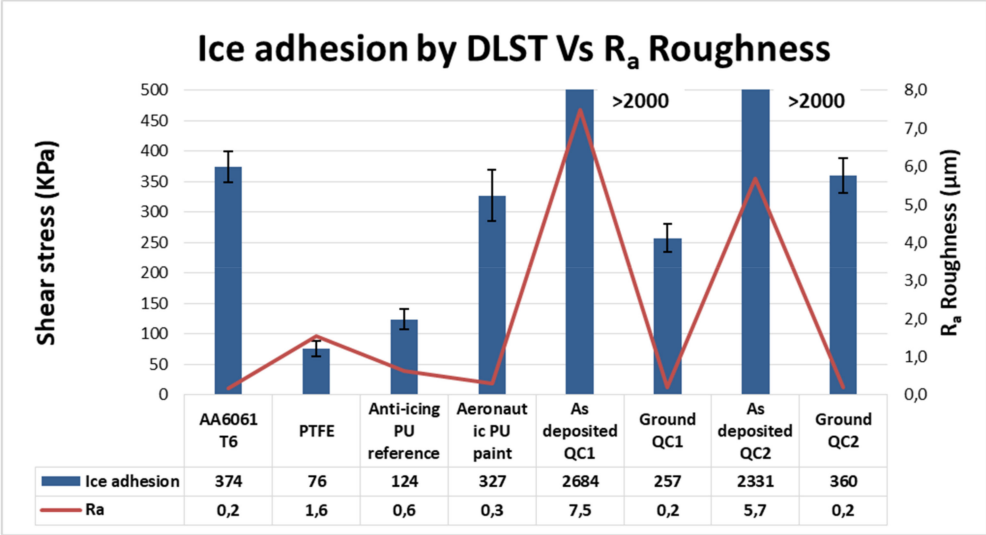

Figure 20. Double lap shear ice adhesion and R_a roughness test results.

3.4. Anti-Icing Performance Discussion

A desired anti-icing material (passive system) should not accrete ice, or at least should retard it, and if ice accretes, detachment should be easy.

None of the studied materials reached completely those objectives, but slight improvement could be seen when some of the previous results are studied together.

In example, PTFE was the best in terms combining both low ice adhesion and accretion (see Figure 21). However, PTFE is not durable, and that is a critical requirement for anti-icing materials to be used on aeronautic components. The anti-icing PU paint Alexit 414-44 proposed by Airbus is also not durable, and exhibits higher ice accretion [71]. On the other hand, the polished QC1 coating, which is expected to be durable given its high hardness, did exhibit lower accretion than the anti-icing PU paint, but higher ice adhesion. This metallic material exhibits relatively good anti-icing properties, in particular when comparing it to uncoated AA6061 T6 and a regular aeronautic PU paint. These results confirm that superhydrophobicity does not always warrantee ice-phobicity. Zou et al. indicated that ice adhesion strength correlates with water contact angle only when the surfaces have similar roughness [26]. In that case, a correlation between roughness and ice adhesion could not be appreciated, due to the different chemical interaction of the different compositions. This is especially notorious in low range roughness (≤1.6 Ra) materials, which are not so affected by the interlocking effect, and the chemical interaction is even higher.

These results suggest that in order to develop anti-icing materials–coatings, it is critical to have access to IWTs, as not simple correlation can be established with any other material property or characteristic.

QC1 is not good enough to consider it as an alternative passive solution in aeronautics, but the showed improvement (especially in ground QC1) respecting to aeronautic references, together with the high hardness, opens the possibility of further development by laser treatment in order to create nano-roughness in combination with slippery liquid-infused porous surfaces (SLIPS) [37].

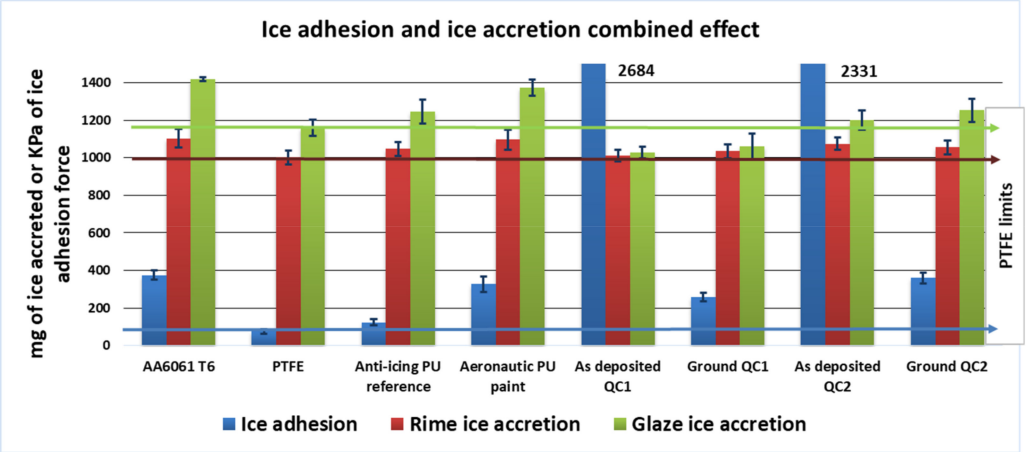

Figure 21. Ice adhesion and ice accretion (Rime and Glaze) results. The horizontal arrows indicate the PTFE values (green for glace ice accretion, red for glaze ice accretion and blue for ice adhesion.

4. Conclusions

The behavior against ice accretion and adhesion of two different anti-stick Al, Fe, Cu and Cr-based QC coatings deposited by the HVOF thermal spray has been studied. The wetting properties, hardness, roughness, ice accretion behavior on an IWT, and ice adhesion by DLST, were determined for these QC coatings, along with other materials used as references (AA6061T6, PTFE and 2 PU paints with and without ice-phobic behavior). The wetting behavior was established by measuring SCAs, ROAs and CAHs on all of the materials. The tests in the IWT were carried out under both glaze and rime ice formation conditions. The ice adhesion test was carried out with ice formed under static conditions. PTFE and ground QC1 exhibited the lowest ice accretion, but differences with the other materials were not very high, especially with glaze ice, where the reduction of accreted ice was of approximately 10% or less. PTFE was also the best for low ice adhesion. None of the tested materials exhibited a sufficiently high anti-icing behavior. However, in terms of ice accretion, QC1 shows very similar values to PTFE, which is considered among the best anti-icing materials, and better than the uncoated Al alloy. QC2 showed just a slight improvement from the AA6061 in ice accretion, in the range of the anti-icing PU paint reference, but higher ice adhesion.

QCs are hard in contrast to PTFE, and therefore more durable, so they can be considered to be used in combination with active systems to reduce their currently high energy requirements. Further improvements by texturing with lasers and by adding slips will be undertaken.

These results are promising, and show that QCs could be a durable alternative in the anti-icing technology, provided that the proper surface texture is achieved. QCs are hard, and therefore difficult to damage when compared to polymeric materials, which are usually employed to confer anti-icing properties. Further testing is required, including durability cycles, the effect of alternative surface treatments such as laser, chemical etching, or the combination with thermal active systems, in order to improve their anti-icing and de-icing ability.

Author Contributions: M.R. carried out the HVOF depositions, and characterized the coatings by Optical and FESEM microscopy; G.P. and M.J. completed the roughness and wetting characterization carried out the ice accretion and ice adhesion tests, and wrote the manuscript with the support and supervision of A.A., leader of the group. All authors have read and agreed to the published version of the manuscript.

Funding: The authors are grateful for the financial support by EC (PHOBIC2ICE, G.A. No.: 690819), as well as the Spanish Ministry of Economy and Competitiveness (HELADA, project No.: TRA2013-48603-C4-4-R).

Acknowledgments: We also thank all members of the Metallic Materials Area at INTA for technical support, in particular A. Fernandez Gamo. Finally, we acknowledge Technology Partners Foundation (Poland), Airbus Group innovations (Germany), and Asociación Industrial de Navarra (AIN) for providing us with the reference materials.

Conflicts of Interest: There are not conflicts of interest in this work.

References

1. Isaac, G.A.; Cober, S.G.; Strapp, J.W.; Korolev, A.V.; Tremblay, A.; Marcotte, D.L. Recent Canadian research on aircraft in-flight icing. *Can. Aeronaut. Space J.* **2001**, *47*, 213–221.
2. Mulherin, N.D.; Haehnel, R.B. Cold Reg. *Res. Eng. Lab. Tech.* **2003**, *3*, 9.
3. Laforte, J.L.; Allaire, M.A.; Laflamme, J. State-of-the-art on power line de-icing. *Atmos. Res.* **1998**, *46*, 143–158. [CrossRef]
4. Ratvasky, T.P.; Barnhart, B.P.; Lee, S. Current methods modeling and simulating icing effects on aircraft performance, stability, control. *J. Aircr.* **2010**, *47*, 201–211. [CrossRef]
5. Mosher, F.R.; Schaum, D.; Herbster, C.; Guinn, T. *Analysis of Causes of Icing Conditions which Contributed to the Crash of Continental Flight 3407*; Embry-Riddle Aeronautical University: Daytona Beach, FL, USA, 2010.
6. Politovich, M.K. Aircraft icing caused by large supercooled droplets. *J. Appl. Meteorol.* **1989**, *28*, 856–868. [CrossRef]
7. Gent, R.W.; Dart, N.P.; Cansdale, J.T. Aircraft icing. Philosophical Transactions of the Royal Society of London. *Ser. A Math. Phys. Eng. Sci.* **2000**, *358*, 2873–2911. [CrossRef]
8. Thomas, S.K.; Cassoni, R.P.; MacArthur, C.D. Aircraft anti-icing and de-icing techniques and modeling. *J. Aircr.* **1996**, *33*, 841–854. [CrossRef]
9. Weisend, N.A., Jr. Inflatable airfoil device. U.S. Patent No. 6,443,394, 3 September 2002.
10. Rutherford, R.B.; Dudman, R.L. Zoned aircraft de-icing system and method. U.S. Patent 6,237,874, 29 May 2002.
11. Petrenko, V.F.; Sullivan, C.R.; Kozlyuk, V.; Petrenko, F.V.; Veerasamy, V. Pulse electro-thermal de-icer (PETD). *Cold Reg. Sci. Technol.* **2011**, *65*, 70–78. [CrossRef]
12. Rudolph, P.K.; Georgefalvy, D. Anti-icing system for aircraft. U.S. Patent No. 5,114,100, 19 May 1992.
13. Gornik, A. Mechanical vibration deicing system. U.S. Patent No. 8,517,313, 27 August 2013.
14. Cornell, J.S.; Pillard, D.A.; Hernandez, M.T. Comparative measures of the toxicity of component chemicals in aircraft deicing fluid. *Environ. Toxicol. Chem. Int. J.* **2000**, *19*, 1465–1472. [CrossRef]
15. Ramakrishna, D.M.; Viraraghavan, T. Environmental impact of chemical deicers–A review. *Water Air Soil Pollut.* **2005**, *166*, 49–63. [CrossRef]
16. Cao, L.; Jones, A.K.; Sikka, V.K.; Wu, J.; Gao, D. Anti-icing superhydrophobic coatings. *Langmuir* **2009**, *25*, 12444–12448. [CrossRef]
17. Honsek, R.; Habashi, W.G.; Aubé, M.S. Eulerian modeling of in-flight icing due to supercooled large droplets. *J. Aircr.* **2008**, *45*, 1290–1296. [CrossRef]
18. Bulte, G.J. Lotus leaf with waterdrops, showing the 'Lotus-effect' [Figure]. Available online: https://commons.wikimedia.org/wiki/File:Lotus_leaf_with_waterdrops.jpg (accessed on 20 March 2020).
19. Latthe, S.S.; Terashima, C.; Nakata, K.; Fujishima, A. Superhydrophobic surfaces developed by mimicking hierarchical surface morphology of lotus leaf. *Molecules* **2014**, *19*, 4256–4283. [CrossRef]
20. Bhushan, B.; Her, E.K. Fabrication of superhydrophobic surfaces with high and low adhesion inspired from rose petal. *Langmuir* **2010**, *26*, 8207–8217. [CrossRef]
21. Liu, K.; Du, J.; Wu, J.; Jiang, L. Superhydrophobic gecko feet with high adhesive forces towards water and their bio-inspired materials. *Nanoscale* **2012**, *4*, 768–772. [CrossRef]
22. He, Y.; Jiang, C.; Cao, X.; Chen, J.; Tian, W.; Yuan, W. Reducing ice adhesion by hierarchical micro-nano-pillars. *Appl. Surf. Sci.* **2014**, *305*, 589–595. [CrossRef]
23. Jung, S.; Dorrestijn, M.; Raps, D.; Das, A.; Megaridis, C.M.; Poulikakos, D. Are superhydrophobic surfaces best for ice-phobicity? *Langmuir* **2011**, *27*, 3059–3066. [CrossRef]
24. Janjua, Z.A.; Turnbull, B.; Choy, K.L.; Pandis, C.; Liu, J.; Hou, X.; Choi, K.S. Performance and durability tests of smart ice-phobic coatings to reduce ice adhesion. *Appl. Surf. Sci.* **2017**, *407*, 555–564. [CrossRef]
25. Hejazi, V.; Sobolev, K.; Nosonovsky, M. From superhydrophobicity to ice-phobicity: Forces and interaction analysis. *Sci. Rep.* **2013**, *3*, 2194. [CrossRef]
26. Zou, M.; Beckford, S.; Wei, R.; Ellis, C.; Hatton, G.; Miller, M.A. Effects of surface roughness and energy on ice adhesion strength. *Appl. Surf. Sci.* **2011**, *257*, 3786–3792. [CrossRef]
27. Matsumoto, K.; Kobayashi, T. Fundamental study on adhesion of ice to cooling solid surface. *Int. J. Refrig.* **2007**, *30*, 851–860. [CrossRef]

28. Dotan, A.; Dodiuk, H.; Laforte, C.; Kenig, S. The relationship between water wetting and ice adhesion. *J. Adhes. Sci. Technol.* **2009**, *23*, 1907–1915. [CrossRef]
29. Bascom, W.D.; Cottington, R.L.; Singleterry, C.R. Ice adhesion to hydrophilic and hydrophobic surfaces. *J. Adhes.* **1969**, *1*, 246–263. [CrossRef]
30. Kulinich, S.A.; Farzaneh, M. How wetting hysteresis influences ice adhesion strength on superhydrophobic surfaces. *Langmuir* **2009**, *25*, 8854–8856. [CrossRef] [PubMed]
31. Meuler, A.J.; Smith, J.D.; Varanasi, K.K.; Mabry, J.M.; McKinley, G.H.; Cohen, R.E. Relationships between water wettability and ice adhesion. *ACS Appl. Mater. Interfaces* **2010**, *2*, 3100–3110. [CrossRef]
32. Jafari, R.; Menini, R.; Farzaneh, M. Superhydrophobic and ice-phobic surfaces prepared by RF-sputtered polytetrafluoroethylene coatings. *Appl. Surf. Sci.* **2010**, *257*, 1540–1543. [CrossRef]
33. Spence, C.F. (Ed.) *AIM-FAR, 1999: Aeronautical Information Manual/Federal Aviation Regulations*; McGraw-Hill Companies: New York, NY, USA, 1998.
34. Wong, T.S.; Kang, S.H.; Tang, S.K.; Smythe, E.J.; Hatton, B.D.; Grinthal, A.; Aizenberg, J. Bioinspired self-repairing slippery surfaces with pressure-stable omniphobicity. *Nature* **2011**, *477*, 443–447. [CrossRef]
35. Bohn, H.F.; Federle, W. Insect aquaplaning: Nepenthes pitcher plants capture prey with the peristome, a fully wettable water-lubricated anisotropic surface. *Proc. Natl. Acad. Sci. USA* **2004**, *101*, 14138–14143. [CrossRef]
36. Kim, P.; Wong, T.S.; Alvarenga, J.; Kreder, M.J.; Adorno-Martinez, W.E.; Aizenberg, J. Liquid-infused nanostructured surfaces with extreme anti-ice and anti-frost performance. *ACS Nano* **2012**, *6*, 6569–6577. [CrossRef]
37. Wilson, P.W.; Lu, W.; Xu, H.; Kim, P.; Kreder, M.J.; Alvarenga, J.; Aizenberg, J. Inhibition of ice nucleation by slippery liquid-infused porous surfaces (SLIPS). *Phys. Chem. Chem. Phys.* **2013**, *15*, 581–585. [CrossRef]
38. Irajizad, P.; Hasnain, M.; Farokhnia, N.; Sajadi, S.M.; Ghasemi, H. Magnetic slippery extreme ice-phobic surfaces. *Nat. Commun.* **2016**, *7*, 1–7. [CrossRef] [PubMed]
39. Rosensweig, R.E. *Ferrohydrodynamics*; Dover Inc.: Mineola, NY, USA, 1997.
40. Irajizad, P.; Farokhnia, N.; Ghasemi, H. Dispensing nano-pico droplets of ferrofluids. *Appl. Phys. Lett.* **2015**, *107*, 191601. [CrossRef]
41. Jung, S.; Tiwari, M.K.; Doan, N.V.; Poulikakos, D. Mechanism of supercooled droplet freezing on surfaces. *Nature communications* **2012**, *3*, 1–8. [CrossRef] [PubMed]
42. Boinovich, L.; Emelyanenko, A.M.; Korolev, V.V.; Pashinin, A.S. Effect of wettability on sessile drop freezing: When superhydrophobicity stimulates an extreme freezing delay. *Langmuir* **2014**, *30*, 1659–1668. [CrossRef]
43. Arianpour, F.; Farzaneh, M.; Kulinich, S.A. Hydrophobic and ice-retarding properties of doped silicone rubber coatings. *Appl. Surf. Sci.* **2013**, *265*, 546–552. [CrossRef]
44. Lv, J.; Song, Y.; Jiang, L.; Wang, J. Bio-inspired strategies for anti-icing. *ACS Nano* **2014**, *8*, 3152–3169. [CrossRef]
45. Menini, R.; Farzaneh, M. Elaboration of Al_2O_3/PTFE ice-phobic coatings for protecting aluminum surfaces. *Surf. Coat. Technol.* **2009**, *203*, 1941–1946. [CrossRef]
46. Laforte, C.; Beisswenger, A. International Workshop on Atmospheric Icing of Structure. In Proceedings of the 10th International Workshop on Atmospheric Icing of Structures, Montréal, QC, Canada, 12–16 June 2005.
47. Golovin, K.; Kobaku, S.P.; Lee, D.H.; DiLoreto, E.T.; Mabry, J.M.; Tuteja, A. Designing durable ice-phobic surfaces. *Sci. Adv.* **2016**, *2*, e1501496. [CrossRef]
48. Boinovich, L.B.; Emelyanenko, A.M.; Emelyanenko, K.A.; Modin, E.B. Modus operandi of protective and anti-icing mechanisms underlying the design of longstanding outdoor ice-phobic coatings. *ACS Nano* **2019**, *13*, 4335–4346. [CrossRef]
49. Dubois, J.M.; Kang, S.S.; Perrot, A. Towards applications of quasicrystals. *Mater. Sci. Eng. A* **1994**, *179*, 122–126. [CrossRef]
50. Brunet, P.; Zhang, L.M.; Sordelet, D.J.; Besser, M.; Dubois, J.M. Comparative study of microstructural and tribological properties of sintered, bulk icosahedral samples. *Mater. Sci. Eng. A* **2000**, *294*, 74–78. [CrossRef]
51. Dubois, J.M.; Goldman, A.I.; Sordelet, D.J.; Thiel, P.A. *New Horizons in Quasicrystals: Research and Applications*; Goldman, A.I., Sordelet, D.J., Thiel, P.A., Eds.; World Scientific Publishing Company: Singapore, 1997; pp. 208–215.
52. Wolf, B.; Bambauer, K.O.; Paufler, P. On the temperature dependence of the hardness of quasicrystals. *Mater. Sci. Eng. A* **2001**, *298*, 284–295. [CrossRef]

53. Kang, S.S.; Dubois, J.M. Pressure-induced phase transitions in quasi-crystals and related compounds. *EPL Europhys. Lett.* **1992**, *18*, 45. [CrossRef]
54. Belin-Ferré, E.; Dubois, J.M.; Fournée, V.; Brunet, P.; Sordelet, D.J.; Zhang, L.M. About the Al 3p density of states in Al–Cu–Fe compounds and its relation to the compound stability and apparent surface energy of quasicrystals. *Mater. Sci. Eng. A* **2000**, *294*, 818–821. [CrossRef]
55. Jenks, C.J.; Thiel, P.A. Quasicrystals: A short review from a surface science perspective. *Langmuir* **1998**, *14*, 1392–1397. [CrossRef]
56. Rivier, N.; Goldman, A.I.; Sordelet, D.J.; Thiel, P.A.; Dubois, J.M. *Physical Properties of Quasicrystals*; World Scientific: Singapore, 1997; pp. 188–199.
57. Belin-Ferre, E. Quasicrystals: Current Topics. *MRS Online Proceedings Library Archive 553* **1998**, 347–358.
58. Van Blaaderen, A. Quasicrystals from nanocrystals. *Nature* **2009**, *461*, 892–893. [CrossRef]
59. Zhang, F.; Robinson, B.W.; de Villiers-Lovelock, H.; Wood, R.J.; Wang, S.C. Wettability of hierarchically-textured ceramic coatings produced by suspension HVOF spraying. *J. Mater. Chem. A* **2015**, *3*, 13864–13873. [CrossRef]
60. Sharifi, N.; Ettouil, F.B.; Moreau, C.; Dolatabadi, A.; Pugh, M. Engineering surface texture and hierarchical morphology of suspension plasma sprayed TiO_2 coatings to control wetting behavior and superhydrophobic properties. *Surf. Coat. Technol.* **2017**, *329*, 139–148. [CrossRef]
61. Qiao, J.H.; Jin, X.; Qin, J.H.; Liu, H.T.; Luo, Y.; Zhang, D.K. A super-hard superhydrophobic Fe-based amorphous alloy coating. *Surf. Coat. Technol.* **2018**, *334*, 286–291. [CrossRef]
62. Koivuluoto, H.; Stenroos, C.; Kylmälahti, M.; Apostol, M.; Kiilakoski, J.; Vuoristo, P. Anti-icing behavior of thermally sprayed polymer coatings. *J. Therm. Spray Technol.* **2017**, *26*, 150–160. [CrossRef]
63. Xi, N.; Liu, Y.; Zhang, X.; Liu, N.; Fu, H.; Hang, Z.; Gao, W. Steady anti-icing coatings on weathering steel fabricated by HVOF spraying. *Appl. Surf. Sci.* **2018**, *444*, 757–762. [CrossRef]
64. Yan, Y.; Jia, Z.; Yang, Y. Preparation and mechanical properties of PTFE/nano-EG composites reinforced with nanoparticles. *Procedia Environ. Sci.* **2011**, *10*, 929–935. [CrossRef]
65. Bonaccurso, E.; Pervier, M.; Pervier, H.; Campazzi, E.; Linassier, G.; Goncalves, E.; Balland, M.; Suel, S. Deliverable 5.4. *STORM-FP7-605180* **2017**.
66. Macdougall, G.; Ockrent, C. Surface energy relations in liquid/solid systems I. The adhesion of liquids to solids and a new method of determining the surface tension of liquids. *Proc. R. Soc. Lond. Ser. A Math. Phys. Sci.* **1942**, *180*, 151–173.
67. SAE Aerospace Recommended Practice (ARP). *Calibration and Acceptance of Icing Wind Tunnels*; SAE: Warrendale, PA, USA, 2015.
68. Goswami, S.; Klaus, S.; Benziger, J. Wetting and absorption of water drops on Nafion films. *Langmuir* **2008**, *24*, 8627–8633. [CrossRef] [PubMed]
69. De Pauw, D.; Dolatabadi, A. Effect of superhydrophobic coating on the anti-icing and deicing of an airfoil. *J. Aircr.* **2017**, *54*, 490–499. [CrossRef]
70. Mangini, D.; Antonini, C.; Marengo, M.; Amirfazli, A. Runback ice formation mechanism on hydrophilic and superhydrophobic surfaces. *Cold Reg. Sci. Technol.* **2015**, *109*, 53–60. [CrossRef]
71. Morita, K.; Okamoto, K.; Aoki, A.; Kimura, S.; Sakaue, H. *Hydrophobic Coating Study for Anti-Icing Aircraft*; No. 2011-38-0010; SAE Technical Paper: Warrendale, PA, USA, 2011.
72. Ozbay, S.; Erbil, H.Y. Ice accretion by spraying supercooled droplets is not dependent on wettability and surface free energy of substrates. *Colloids Surf. A Physicochem. Eng. Asp.* **2016**, *504*, 210–218. [CrossRef]
73. Sharifi, N.; Dolatabadi, A.; Pugh, M.; Moreau, C. Anti-icing performance and durability of suspension plasma sprayed TiO_2 coatings. *Cold Reg. Sci. Technol.* **2019**, *159*, 1–12. [CrossRef]
74. ISO. *Atmospheric Icing of Structures*; International Standard; ISO: Geneva, Switzerland, 2001; p. 12494.
75. Antonini, C.; Innocenti, M.; Horn, T.; Marengo, M.; Amirfazli, A. Understanding the effect of superhydrophobic coatings on energy reduction in anti-icing systems. *Cold Reg. Sci. Technol.* **2011**, *67*, 58–67. [CrossRef]
76. Ferrick, M.G.; Mulherin, N.D.; Haehnel, R.B.; Coutermarsh, B.A.; Durell, G.D.; Tantillo, T.J.; Welser, E.S.; Cano, R.J.; Smith, R.J.; Martinez, E.C. *Double Lap Shear Testing of Coating Modified Ice Adhesion to Liquid Oxygen Food Line Bracket, Space Shuttle External Tank*; No. ERDC/CRREL-TR-06-11; Engineering Research and Development Center Hanover nh cold Regions Research and Engineering Lab: Hanover, NH, USA, 2006.

77. Kimura, S.; Yamagishi, Y.; Sakabe, A.; Adachi, T.; Shimanuki, M. *A New Surface Coating for Prevention of Icing on Airfoils*; No. 2007-01-3315; SAE Technical Paper: Warrendale, PA, USA, 2007.
78. Menini, R.; Ghalmi, Z.; Farzaneh, M. Highly resistant ice-phobic coatings on aluminum alloys. *Cold Reg. Sci. Technol.* **2011**, *65*, 65–69. [CrossRef]
79. Karmouch, R.; Coudé, S.; Abel, G.; Ross, G.G. Ice-phobic PTFE coatings for wind turbines operating in cold climate conditions. In Proceedings of the 2009 IEEE Electrical Power & Energy Conference (EPEC), Montreal, QC, Canada, 22–23 October 2009; pp. 1–6.
80. Chen, J.; Liu, J.; He, M.; Li, K.; Cui, D.; Zhang, Q.; Song, Y. Superhydrophobic surfaces cannot reduce ice adhesion. *Appl. Phys. Lett.* **2012**, *101*, 111603. [CrossRef]
81. Yeong, Y.H.; Loth, E.; Sokhey, J.; Lambourne, A. *Ice Adhesion Performance of Superhydrophobic Coatings in Aerospace Icing Conditions*; No. 2015-01-2120; SAE Technical Paper: Warrendale, PA, USA, 2015.